Fibers and Polymers 2003, Vol.4, No.2, 77-83

Constitutive Equations Based on Cell Modeling Method for 3D Circular Braided Glass Fiber Reinforced Composites

Wonoh Lee, Ji Hoon Kim, Heon-Jung Shin[1], Kwansoo Chung*, Tae Jin Kang, and Jae Ryoun Youn

School of Materials Science and Engineering, Research Institute of Advanced Materials, Seoul National University, 56-1, Shinlim-dong, Kwanak-gu, Seoul 151-742, Korea

[1]LG Chem. Tech Center, 84, Jang-dong, Yuseong-gu, Daejeon 305-343, Korea

(Received May 12, 2003; Revised June 5, 2003; Accepted June 10, 2003)

Abstract: The cell modeling homogenization method to derive the constitutive equation considering the microstructures of the fiber reinforced composites has been previously developed for composites with simple microstructures such as 2D plane composites and 3D rectangular shaped composites. Here, the method has been further extended for 3D circular braided composites, utilizing B-spline curves to properly describe the more complex geometry of 3D braided composites. For verification purposes, the method has been applied for orthotropic elastic properties of the 3D circular braided glass fiber reinforced composite, in particular for the tensile property. Prepregs of the specimen have been fabricated using the 3D braiding machine through RTM (resin transfer molding) with epoxy as a matrix. Experimentally measured uniaxial tensile properties agreed well with predicted values obtained for two volume fractions.

Keywords: 3D circular braided glass fiber reinforced composites, Constitutive equations, Cell modeling method, Homogenization, Multi-level meshing, RTM (resin transfer molding)

Introduction

Multi-axial fiber reinforced composites have been applied to various industrial fields, because of their remarkable material properties such as high damage tolerance, fatigue and impact resistances, and interlaminar failure reduction as well as their practicality. Recently, the application has been further extended to automotive and airspace industries. Among various methods fabricating multi-axial fiber reinforced composites, the braiding technique has the advantage of convenient handling, which enables manufacturers to fabricate composites in various shapes such as I-beam, H-beam and even tube shapes.

Because the physical property of the composite is dependent on its geometric structure as well as the material property of composing materials, the geometric modeling to describe microstructures of fiber reinforced composites is necessary to understand their properties and therefore also to design composites. Early works on the geometric modeling of fiber reinforced composites were limited to 2D plane composites and 3D rectangular shaped composites, in which yarn paths were assumed straight[1,2]. As for rectangular braided composites, Li and El Shiekh[3] proposed the unit cell model by considering the carrier movement, but they used straight yarn paths having circular yarn cross sections. Pandey and Hahn[4] suggested the model, which can represent the volume fraction change by taking account of yarn crimping and jamming effects. Chen *et al.*[5] and Byun and Chou[6] considered the unit cell, which is divided into the surface cell and the inner cell. For 3D circular braided composites, Hammad *et al.*[7] projected the 3D unit cell into the 2D plane for simplification and elliptic curves were assumed for yarn paths.

The efforts to predict mechanical properties of composites based on unit cell geometries are found in various works including the one by Du and Ko[8], which showed that braided composites have more strength than laminated composites. Masters *et al.*[9] proposed the diagonal brick model, but using straight yarn paths which unrealistically penetrate each other. Later, Byun[10] introduced the bent yarn structure to avoid penetrations of yarns. Bigaud and Hamelin[11,12] developed the cell modeling method considering the equilibrium and strain continuity conditions, saving a significant amount of computation time and memory resources, but the effort was limited to 3D rectangular shaped composites.

Here, the cell modeling method has been further extended for 3D circular braided composites, using B-spline curves and elliptic yarn cross sections to describe the more realistic geometry of 3D braided composites. Constitutive equations for 3D circular braided composites have been derived based on the homogenization technique using the cell modeling method. For verification purposes, application has been made for elastic tensile properties of the 3D circular braided glass fiber reinforced composite. Prepregs of 3D circular braided glass fiber reinforced composite have been fabricated using the 3D braiding machine through RTM with epoxy as a matrix. The uniaxial tensile test was performed for two volume fractions, for comparison with predictions made from the constitutive equation developed.

*Corresponding author: chungch@gong.snu.ac.kr

Geometric Modeling

For composite materials, a unit cell is defined as a repeating geometric structure, which can represent material properties of composites. Therefore, 3D circular braided composites are composed of numerous unit cells and one unit cell is also considered made up of several basic cells which share the same morphological structure with the unit cell. The schematic shape of the unit cell in the 3D circular braided composite is shown in Figure 1. The structure of the basic cell depends on yarn paths passing through the basic cell and Figure 2 shows a schematic view of a basic cell, in which two yarn paths cross each other in the basic cell. The unit cell can be typically divided into three kinds of basic cells: the inner cell, the outer surface cell and the inner surface cell as shown in Figure 3.

In order to define the yarn geometry, it is convenient to introduce a local coordinate system embedded on the yarn. If the yarn path is regarded as a 3D curve, three orthogonal vectors are defined at any position on the yarn path: the tangent vector t, the principal normal vector n and the binormal vector b. Therefore, the direction of the yarn path can be determined considering the tangent vector, and the principal normal vector and the binormal vector become two orthogonal axes on the yarn cross section, which is normal to the yarn path. Figure 4 shows the local coordinate system with the three orthogonal vectors defined for the yarn path and the

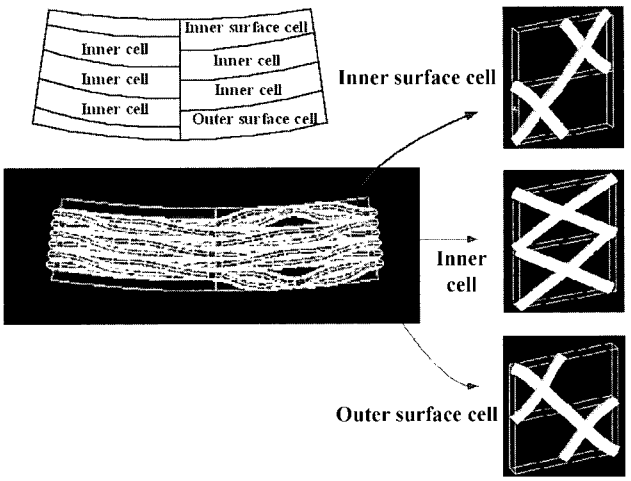

Figure 3. Three typical basic cells in the unit cell.

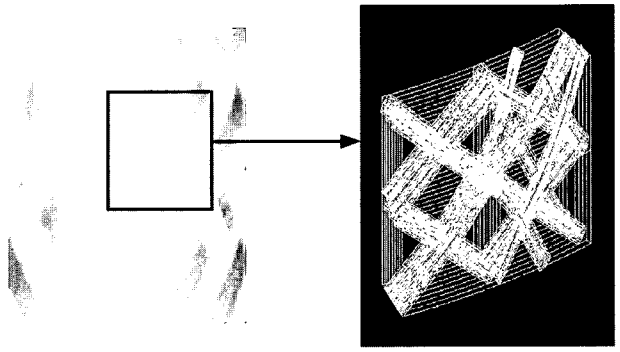

Figure 1. A schematic view of the unit cell.

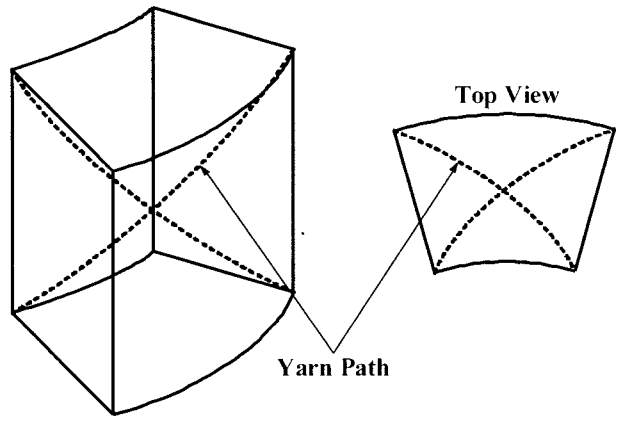

Figure 2. A schematic view of the basic cell.

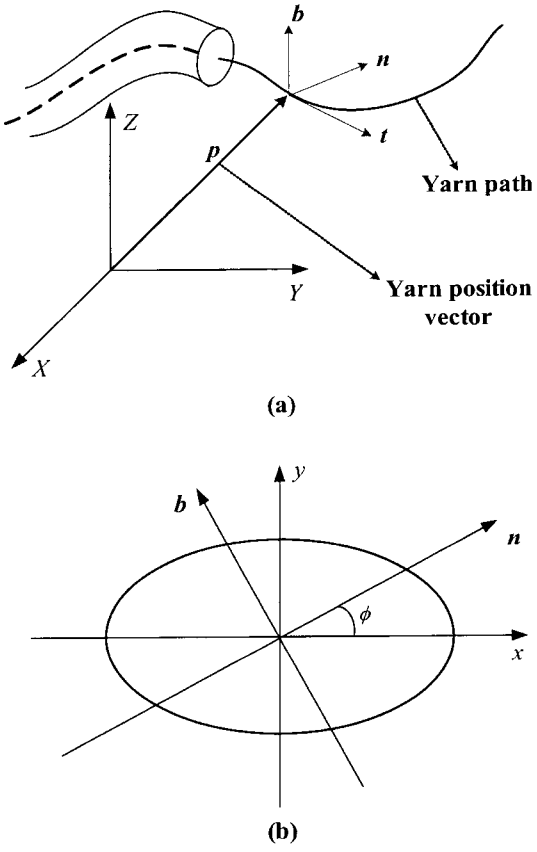

Figure 4. (a) The local coordinate system with the orthogonal vectors defined on the yarn and (b) the (assumed elliptic) cross-sectional shape.

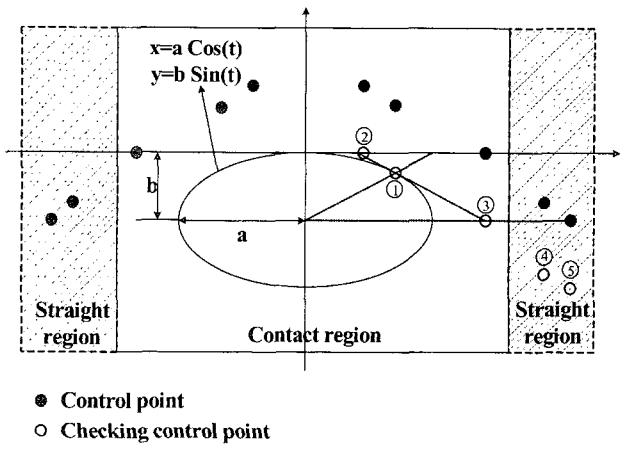

Figure 5. Control points for the B-spline yarn path.

cross-sectional shape. As for the yarn cross-section, elliptic and lenticular contours are generally used for the simplification. Figure 4 shows an exemplary elliptic cross-section with the major and minor axes of the ellipse and the principal normal and binormal vectors.

In order to describe the curved yarn path (supposed by, the path of the cross-sectional center), the B-spline curve is used here, which has 10 control points and 3rd order knots. Figure 5 shows how to determine 10 control points around the region where two yarns cross each other. This region is divided into the contact region and the straight region considering the yarn thickness and the distance between neighboring yarns. After determining the contact and straight regions, the checking control points ~ are obtained such that the direction of the convexity of the yarn does not change. And then, all 10 control points are determined by translating the checking control points ~ along the minor axis and considering the symmetry of the yarn path with respect to the minor axis and finally, the yarn path is obtained as a B-spline curve as shown in Figure 6. Figure 7 shows the top view of yarns crossing each other with the crossing angle ψ. Here, the line AB (and A'B') are the top view of the cross-section of one

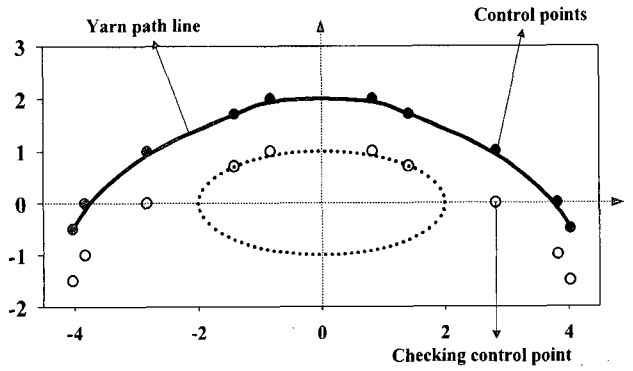

Figure 6. The B-Spline yarn path.

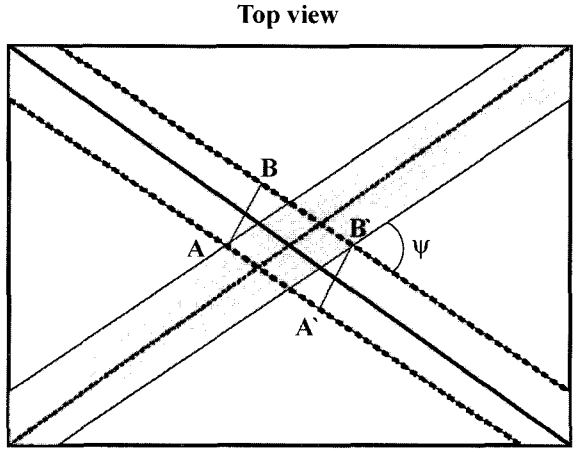

Figure 7. The top view of yarns crossing each other.

member. The figure illustrates the one end A of the cross-section makes earlier contact with the other yarn than the other end B does unless $\psi = 90^{\circ}$ (or 180°) so that the angle ϕ in Figure 4 changes as two yarns cross over each other, which was also taken care of in this work. Through this procedure, the basic cell and the unit cell of the 3D circular braided composite are obtained as schematically shown in Figures 8 and 9 respectively.

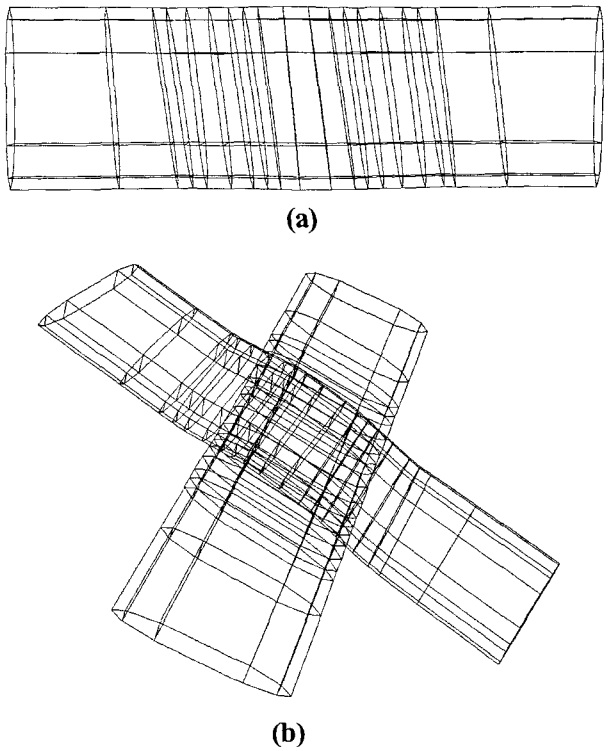

Figure 8. (a) The schematic views of the yarn shape and (b) the basic cell.

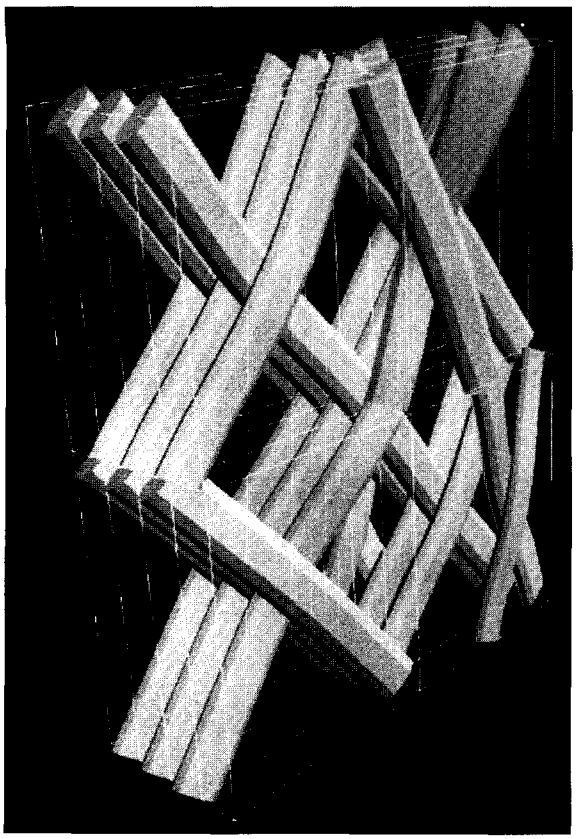

Figure 9. The unit cell of the 3D circular braided composite.

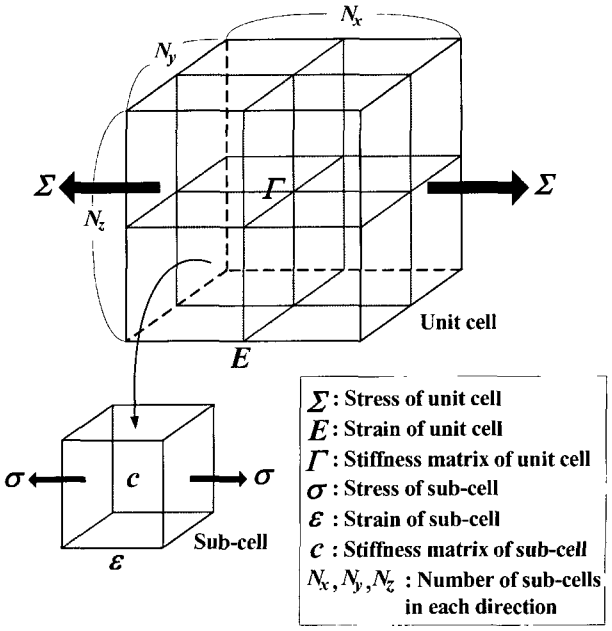

Figure 10. The unit cell subdivided into $N_xN_yN_z$ sub-cells.

Mechanical Modeling

The constitutive equation of fiber reinforced composites can be derived considering their geometric structures using homogenization techniques. Because the homogenization based on multi-level meshing demands so much computation time and memory resources, it is difficult to apply the homogenization for the case of unit cell structures with complex geometry. In order to overcome this disadvantage, the cell modeling method has been introduced. In the cell modeling method, the unit cell is subdivided into several sub-cells and the stiffness matrix of the unit cell is determined considering the force equilibrium and strain continuity conditions between the unit cell and the sub-cell[11,12].

Assuming that the 3D circular braided composite is an orthotropic elastic material and the size of unit cell is small enough compared to the whole composite structure, consider a unit cell, which is subdivided into $N_xN_yN_z$ sub-cells having the same shape and size as shown in Figure 10. Now, the constitutive relations of the unit cell and the sub-cell are, respectively,

$$\boldsymbol{\Sigma} = \boldsymbol{\Gamma E} \quad \text{and} \quad \boldsymbol{\sigma} = \boldsymbol{c\varepsilon}. \tag{1}$$

Here, $\boldsymbol{\Sigma}$, $\boldsymbol{\Gamma}$, and $\boldsymbol{E}$ are stress tensor, stiffness matrix and strain tensor of the unit cell and $\boldsymbol{\sigma}$, $\boldsymbol{c}$, and $\boldsymbol{\varepsilon}$ are those of the sub-cell. The relationship between $\boldsymbol{\Gamma}$ and $\boldsymbol{c}$ is obtained after the relationship between $\boldsymbol{E}$ and $\boldsymbol{\varepsilon}$ is considered based on the equilibrium condition and the strain continuity. Note that because $\boldsymbol{\Sigma}$ is the average of the local stresses $\boldsymbol{\sigma}$.

The strain continuity condition requires that the global strain $\boldsymbol{E}$ is the average of local strain $\boldsymbol{\varepsilon}$ of each sub-cell under the condition that the size of the sub-cell is the same. Therefore,

$$\begin{aligned}
\sum_{i}^{N_x} \varepsilon_{xx}^{i,j,k} &= N_x E_{xx} \quad \text{for all } (j,k) \\
\sum_{j}^{N_y} \varepsilon_{yy}^{i,j,k} &= N_y E_{yy} \quad \text{for all } (i,k) \\
\sum_{k}^{N_z} \varepsilon_{zz}^{i,j,k} &= N_z E_{zz} \quad \text{for all } (i,j) \\
\sum_{j}^{N_y}\sum_{k}^{N_z} \varepsilon_{yz}^{i,j,k} &= N_y N_z E_{yz} \quad \text{for all } (i) \\
\sum_{i}^{N_x}\sum_{k}^{N_z} \varepsilon_{xz}^{i,j,k} &= N_x N_z E_{xz} \quad \text{for all } (j) \\
\sum_{i}^{N_x}\sum_{j}^{N_y} \varepsilon_{xy}^{i,j,k} &= N_x N_y E_{xy} \quad \text{for all } (k)
\end{aligned} \tag{2}$$

where (i, j, k) are the indices to identically each sub-cell. There are $N_yN_z + N_xN_z + N_xN_y + N_x + N_y + N_z$ equations in equation (2).

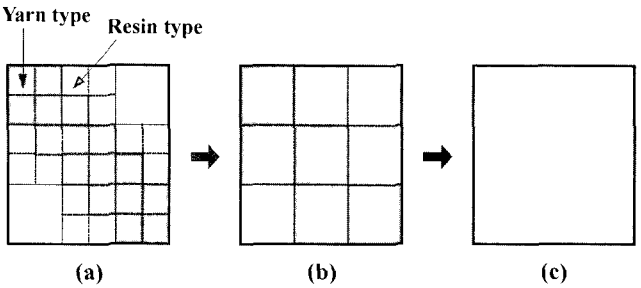

Figure 11. Application of the cell modeling method in multi-levels: (a) lowest level, (b) intermediate level, and (c) continuum level.

The force equilibrium condition gives the stress relationship between adjacent sub-cells having the same contact surface area. Therefore,

$$\begin{aligned}
\sigma_{xx}^{i,j,k} &= \sigma_{xx}^{i+1,j,k} \\
\sigma_{yy}^{i,j,k} &= \sigma_{yy}^{i,j+1,k} \\
\sigma_{zz}^{i,j,k} &= \sigma_{zz}^{i,j,k+1} \\
\sigma_{yz}^{i,j,k} &= \sigma_{yz}^{i,j+1,k} = \sigma_{yz}^{i,j,k+1} \\
\sigma_{xz}^{i,j,k} &= \sigma_{xz}^{i,j,k+1} = \sigma_{xz}^{i+1,j,k} \\
\sigma_{xy}^{i,j,k} &= \sigma_{xy}^{i+1,j,k} = \sigma_{xy}^{i,j+1,k}
\end{aligned} \tag{3}$$

for all (i, j, k) except on boundaries.

Equation (3) gives $6N_xN_yN_z - N_yN_z - N_xN_z - N_xN_y - N_x - N_y - N_z$ equations. After considering the linear elastic constitutive equations of the sub-cell shown in equation (1), equation (3) becomes

$$\begin{aligned}
&(c_{11}^{i,j,k}\varepsilon_{xx}^{i,j,k} + L + c_{16}^{i,j,k}\varepsilon_{xy}^{i,j,k}) \\
&-(c_{11}^{i+1,j,k}\varepsilon_{xx}^{i+1,j,k} + L + c_{16}^{i+1,j,k}\varepsilon_{xy}^{i+1,j,k}) = 0
\end{aligned} \tag{4}$$

for all (i, j, k) except on boundaries.

Note here that the orthotropic elastic stiffness coefficients $\boldsymbol{c}^{i,j,k}$ for the resin and composing yarns. Now, equations (2) and (3) are rewritten as,

$$[\boldsymbol{L}][\bar{\boldsymbol{\varepsilon}}] = [\boldsymbol{M}][\boldsymbol{E}]$$

$$\text{where } [\bar{\boldsymbol{\varepsilon}}] = \begin{bmatrix} [\boldsymbol{\varepsilon}]^{1,1,1} \\ M \\ [\boldsymbol{\varepsilon}]^{i,j,k} \\ M \\ [\boldsymbol{\varepsilon}]^{N_x,N_y,N_z} \end{bmatrix}, \quad [\boldsymbol{\varepsilon}]^{i,j,k} = \begin{bmatrix} \varepsilon_{xx}^{i,j,k} \\ \varepsilon_{yy}^{i,j,k} \\ M \\ \varepsilon_{xy}^{i,j,k} \end{bmatrix}, \quad [\boldsymbol{E}] = \begin{bmatrix} E_{xx} \\ E_{yy} \\ M \\ E_{xy} \end{bmatrix}. \tag{5}$$

Here, $[\boldsymbol{\varepsilon}]^{i,j,k}$ and $[\boldsymbol{E}]$ are 6×1 matrices and $[\bar{\boldsymbol{\varepsilon}}]$ becomes a $6N_xN_yN_z \times 1$ matrix. Besides, $[\boldsymbol{M}]$ is a $6N_xN_yN_z \times 6$ matrix and $[\boldsymbol{L}]$ is a $6N_xN_yN_z \times 6N_xN_yN_z$ matrix. When solved with respect to $[\bar{\boldsymbol{\varepsilon}}]$, equation (5) becomes

$$[\bar{\boldsymbol{\varepsilon}}] = [\boldsymbol{L}]^{-1}[\boldsymbol{M}][\boldsymbol{E}] = [\bar{\boldsymbol{K}}][\boldsymbol{E}] \tag{6}$$

where $[\bar{\boldsymbol{K}}]$, $6N_xN_yN_z \times 6$ matrix, can be expressed as a set of 6×6 element matrices $[\boldsymbol{K}]^{i,j,k}$ as

$$[\bar{\boldsymbol{K}}] = \begin{bmatrix} [\boldsymbol{K}]^{1,1,1} \\ M \\ [\boldsymbol{K}]^{i,j,k} \\ M \\ [\boldsymbol{K}]^{N_x,N_y,N_z} \end{bmatrix} \tag{7}$$

In equation (6), the relationship between the local strain $\boldsymbol{\varepsilon}$ of the sub-cell and the global strain $\boldsymbol{E}$ of the unit cell is obtained as

$$[\boldsymbol{\varepsilon}]^{i,j,k} = [\boldsymbol{K}]^{i,j,k}[\boldsymbol{E}]. \tag{8}$$

The global stress $\boldsymbol{\Sigma}$ of the unit cell is defined as the average local stress $\boldsymbol{\sigma}$ of the sub-cell; i.e.,

$$[\Sigma] = \frac{\sum_{i,j,k}^{N_x,N_y,N_z} [\boldsymbol{\sigma}]^{i,j,k}}{N_xN_yN_z}$$

$$\text{where } [\boldsymbol{\Sigma}] = \begin{bmatrix} \Sigma_{xx} \\ \Sigma_{yy} \\ M \\ \Sigma_{xy} \end{bmatrix}, \quad [\boldsymbol{\sigma}]^{i,j,k} = \begin{bmatrix} \sigma_{xx}^{i,j,k} \\ \sigma_{yy}^{i,j,k} \\ M \\ \sigma_{xy}^{i,j,k} \end{bmatrix} \tag{9}$$

After considering equations (1) and (8), the global stiffness matrix $\boldsymbol{\Gamma}$ is finally obtained from equation (9) as

$$[\boldsymbol{\Gamma}] = \frac{\sum_{i,j,k}^{N_x,N_y,N_z} [\boldsymbol{c}]^{i,j,k}[\boldsymbol{K}]^{i,j,k}}{N_xN_yN_z} \tag{10}$$

where $[\boldsymbol{\Gamma}]$ is a 6×6 matrix. Note that $[\boldsymbol{K}]^{i,j,k}$ already includes the components of $[\boldsymbol{c}]^{i,j,k}$.

Note that the cell modeling method based on sub-cells having the same shape and size can also be effectively applied for the case where the size and shape of the sub-cells are not the same, by introducing the multi-level scheme shown in Figure 11. In this example case made of three levels, the sub-cells at the intermediate and continuum levels have the same size and shape but the sub-cells of the

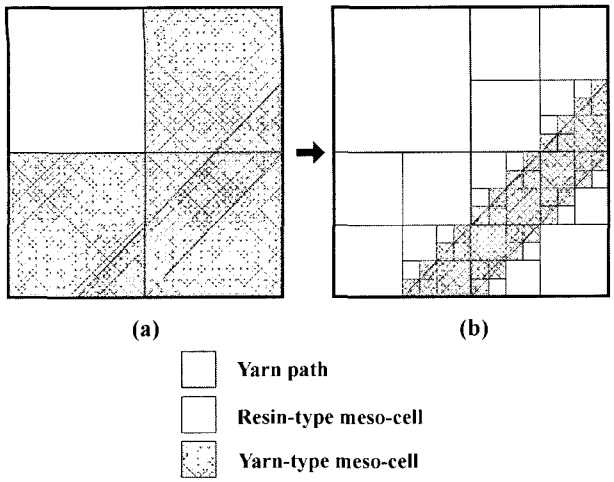

Figure 12. An example of multi-level meshing considering the yarn path.

intermediate level are selectively further divided into smaller meso-cells considering the location of composing materials: the resin-type meso-cell and the yarn type meso-cell with dark color in Figure 11(a). Now, the cell modeling method is applied only for the sub-cell having the four meso-cells in Figure 11(a) to obtain the sub-cell stiffness. This sub-cell stiffness is then used in the intermediate level to calculate the continuum level stiffness using the cell modeling method. In this procedure, the orthogonal property of the yarn is accounted for considering the local direction of the yarn path. An example of the multi-level meshing considering the yarn path is shown in Figure 12.

Experiment and Results

The 3D circular braided glass fiber reinforced composite preform was fabricated using the 3D braiding machine having 2014 carriers and 104 pistons. The 4 step cycle carrier movement is schematically shown in Figure 13. Figure 14 shows the completed preform was placed RTM process using the epoxy resin with a curing agent. It tooks about 10 hours to inject the resin into the RTM cast and then, the 3D circular braided composite was obtained after curing in the oven at 130°C for 90 min. In order to determine the yarn volume fraction of the 3D circular braided composite, the mass of the glass fiber was measured after the resin was removed in combustion in the furnace at 600 °C for 3 hours.

To verify the performance of the constitutive equation derived using the geometric and cell modeling methods, the predicted uniaxial tensile properties of the 3D circular braided composite were compared with experiments for the axial and transverse directions. Figure 15 shows the tensile test specimen. The measured and predicted Young's moduli are compared in Figure 16 for two volume fractions. The figure shows that the predicted values agree well with

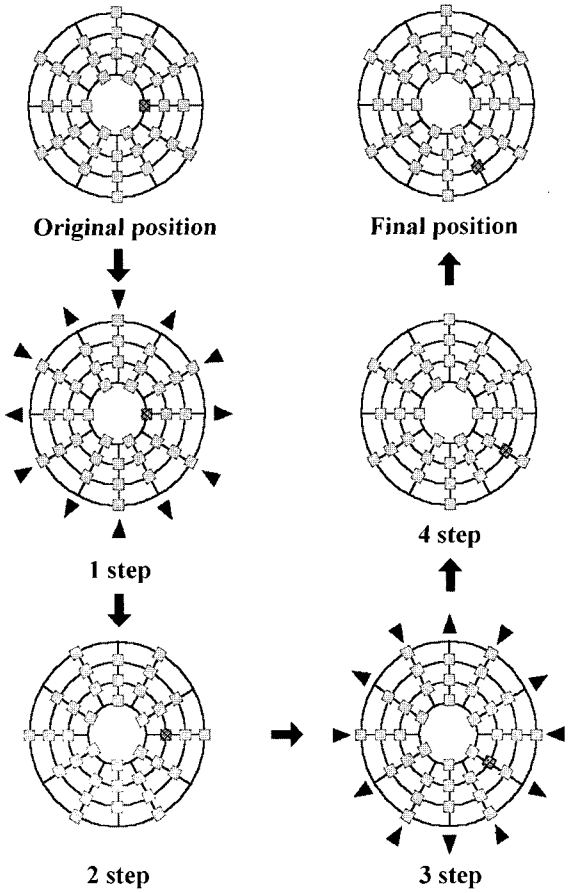

Figure 13. A schematic view of the 4 step cycle carrier movement in the 3D circular braiding machine.

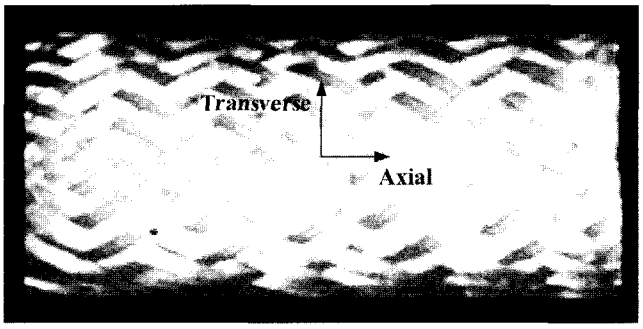

Figure 14. The 3D circular braided glass fiber perform and its axial direction.

experimental results in each direction and volume fraction.

Summary

The homogenization technique to derive the constitutive equations of fiber reinforced composites based on the cell modeling method has been previously developed for composites with simple geometry and the method was further extended

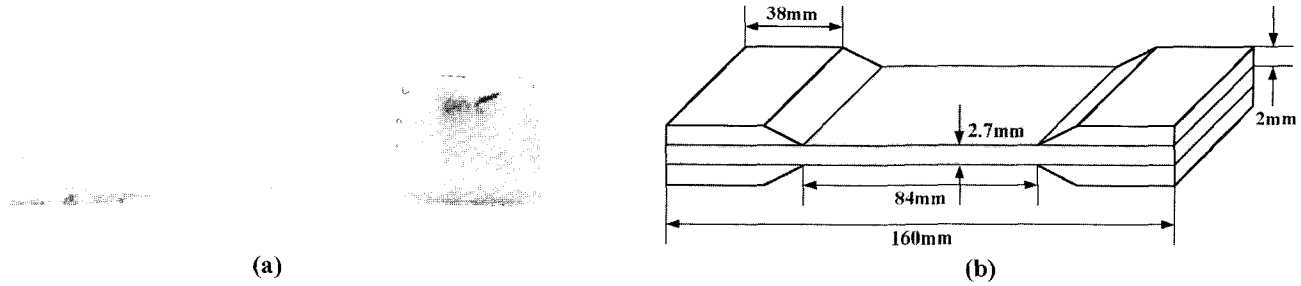

Figure 15. (a) The 3D circular braided composite specimen and (b) its dimension for the tensile test.

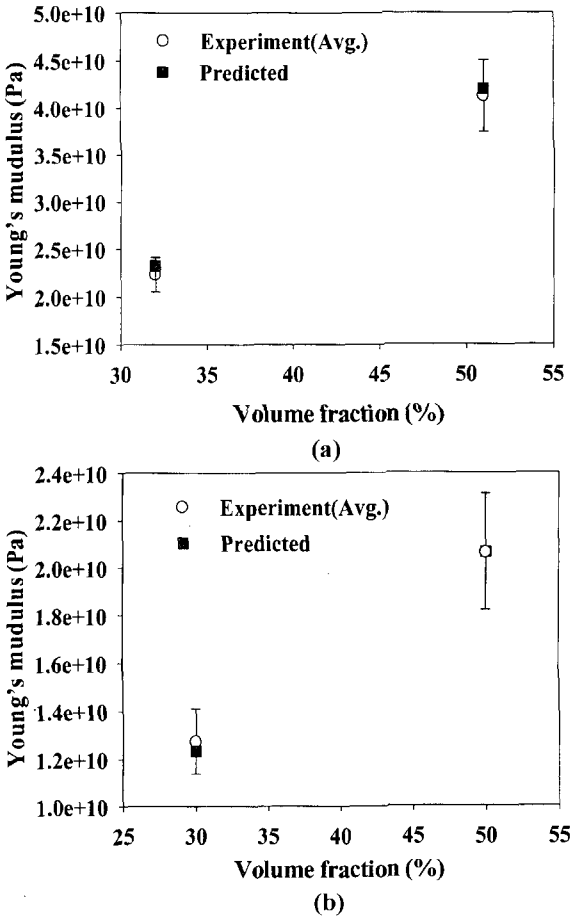

Figure 16. Comparison of Young's moduli (a) in the axial direction and (b) in the transverse direction for the uniaxial tensile test.

in this work for the 3D circular braided composite having more complex geometry. For the geometric modeling of the unit cell, B-spline curves were introduced. For verification purposes, prepregs of 3D circular braided glass fiber reinforced composites were fabricated using the 3D braiding machine through RTM and the predicted and measured Young's moduli were measured in the axial and transverse directions for two volume fractions. The predicted values obtained from the constitutive equation agreed well with experimental results.

Acknowledgement

This work was supported by the Ministry of Science and Technology in Korea through the National Research Laboratory for which the authors feel so thankful.

References

1. F. K. Ko, *J. Comp. Mater.*, **20**, 392 (1986).
2. C. L. Ma, J. M. Yang, and T. W. Chou, *J. Comp. Mater.*, **20**, 404 (1986).
3. W. Li and A. El Shiekh, *SAMPE Quart.*, 22 (1988).
4. P. Pandey and H. T. Hahn, *Comp. Sci. Tech.*, **56**, 161 (1996).
5. L. Chen, X. M. Tao, and C. L. Choy, *Comp. Sci. Tech.*, **59**, 391 (1999).
6. J. H. Byun and T. W. Chou, *Comp. Sci. Tech.*, **56**, 235 (1996).
7. M. Hammad, M. El Messery, and A. El Shiekh, *SAMPE Quart.*, 114 (1991).
8. G. Du and F. K. Ko, *J. Reinforced Plast. Comp.*, **12**, 752 (1993).
9. J. E. Masters, R. L. Foye, C. M. Pastore, and Y. A. Gowayed, *J. Comp. Tech. Res.*, **15**, 112 (1993).
10. J. H. Byun, *Comp. Sci. Tech.*, **60**, 705 (2000).
11. D. Bigaud and P. Hamelin, *Sci. Eng. Comp. Mat.*, **7**, 292 (1998).
12. D. Bigaud and P. Hamelin, *Comp. Tech. Mat.*, 73 (2000).